High Voltage

WILEY

ORIGINAL RESEARCH OPEN ACCESS

Electrical Breakdown Analysis of Emerging Oil–Paper Insulation Systems

Yue Xu[1] | Soori Tejaswi[2] | Kent Davey[1] | Qian Zhang[3] | Vaibhav Bahadur[2] | Junyong Zhu[4] | Robert Hebner[1,2] | Zhedong Han[5] | Felix Lin[5] | Liangbing Hu[3]

[1]Center for Electromechanics, The University of Texas at Austin, Austin, Texas, USA | [2]Walker Department of Mechanical Engineering, University of Texas at Austin, Austin, Texas, USA | [3]Department of Electrical and Computer Engineering, Yale University, New Haven, Connecticut, USA | [4]U.S. Department of Agriculture (USDA) Forest Products Laboratory, Madison, Wisconsin, USA | [5]Department of Materials Science and Engineering, University of Maryland, College Park, Maryland, USA

Correspondence: Yue Xu (y.xu@cem.utexas.edu)

Received: 13 June 2025 | **Revised:** 24 September 2025 | **Accepted:** 14 November 2025

Associate Editor: Jianying Li

ABSTRACT

This investigation addresses the effect of particulate additives on the electrical breakdown strength of the oil impregnated insulation paper system. The morphological complexity is addressed by converting data from scanning electron microscope images to a data set suitable for numerical simulation analysis. Then, by using the conventional oil-triggered breakdown assumption, the breakdown strength of the proposed hybrid insulation system was calculated. As a result, it demonstrates that the introduction of particles can redefine the electric field distribution in the hybrid insulation system under study. Consequently, a higher applied voltage is needed for the electrical breakdown to occur in the hybrid system with proper selection and addition of particles. This analysis method builds on the existing understanding of the electrical breakdown phenomena for oil impregnated insulation paper system, explains recent experimental data and supports improvements of material design in the future.

1 | Introduction

Improving the through-plane thermal conductivity of the insulation system while maintaining its electrical properties is a topic of broad interest in insulation material development [1–4]. For the oil-impregnated insulation paper systems (oil–cellulose systems), emerging technology offers the capability to develop material systems with thermal, electrical and mechanical properties not available currently. Recent research showed the benefit of adding boron nitride (BN) particles into cellulosic material to produce a novel oil-impregnated BN paper system (oil–BN–cellulose system) [5]. Based on previous studies of novel insulation material development, this research is intended to improve insulation material engineering by enhancing the understanding of the initial electrical breakdown process in such oil–BN–cellulose systems.

Earlier studies showed that by adding nanoparticles to a polymer, insulating oil or cellulose-based material, the electrical breakdown strength, voltage endurance, mechanical properties and thermal stability of the material can be improved depending on the types and loadings of nanoparticles [6–9]. However, the thorough-plane thermal conductivity was not reported presumably because the enhancement in thermal conductivity by the nanoparticles was too small to have a practical impact [10–12].

Recent research explored the addition of both micro and nano particles as fillers into epoxy composites to achieve adequate electrical and thermal behaviour [13]. However, the results showed that the electrical breakdown strength enhancement in epoxy composites was limited by two key factors. First, adding filler material increased the electric field (E-field) strength in the polymer matrix instead of the fillers due to the mismatch of relative permittivity values between the polymer and filler material. Second, defects (voids or weak cross-linking zones) were introduced into the polymer matrix, especially under high loadings of micro- and nano-particles.

For oil–cellulose systems, previously published modelling of the electrical breakdown analysis focused on the breakdown mechanism for pure insulation oil [14, 15]. Later studies developed analytic models to explain the experimental data for the oil–cellulose system by considering factors such as the electric field distribution and distortion in the hybrid system after doping the insulation oil with fillers, the space charge and charge distribution under DC excitation, the dynamics of insulation liquid and the electron injection by point electrodes [16–19]. However, these models did not consider morphology variations and assumed a homogeneous paper structure by using an averaging paper morphology model.

Research on the electrical breakdown of an oil–cellulose insulation system under the influence of high frequency electromagnetic pulse (EMP) produced by the denotation of a nuclear weapon using material properties that initiated breakdown in the cellulose fibres [20, 21]. These 3D models predicted the electrical breakdown strength of the insulation paper, but the breakdown modelling was based on an arbitrary morphology under certain test conditions and did not include fillers such as BN [21]. The conditions described in [20, 21] did not match the operation conditions in power transformers, although the references motivated this research and provided useful information for simulation settings.

In summary, in the conventional oil-impregnated insulation paper system, oil displaces air in the paper to increase the electrical breakdown strength. Detailed electrical breakdown dynamics are not well documented because of the complexity of insulation systems consisting of a mixture of materials. The increase in electrical breakdown strength by going from a porous insulation paper with many air voids to an oil–cellulose system supports the hypothesis that electrical breakdown is initiated when the electric field strength in the lowest breakdown component reaches its own electrical breakdown strength. This hypothesis was reinforced by literature showing that a change in the dielectric properties of the oil and the cellulose can move the electrical breakdown initiation into cellulous region under some excitation conditions [21]. Furthermore, research also showed using oil doped with nanoparticles increased electrical breakdown strength of an oil–cellulose system due to the increasing breakdown strength of the insulation oil [16, 22].

Recently, BN particles with nominal diameter of 25 μm were added to cellulosic material and form a novel oil–BN–cellulose system to significantly enhance its through-plane thermal conductivity. The experimental data showed that the electrical breakdown strength of this proposed oil–BN–cellulose system was also increased [5]. The result extends the existing knowledge on enhancing electrical breakdown strength by adding micro- or nano-particles into paper of oil-impregnated insulation paper systems as long as they are properly applied.

To understand the mechanism of the enhancement in electrical breakdown strength for the proposed oil–BN–cellulose hybrid insulation system and to continue improve its electrical breakdown performance for future material design and optimization, a scanning electron microscopy (SEM) image-based modelling and simulation approach which can capture the morphology of the system and predict its micro-scale behaviour is developed. Different from earlier research of electrical breakdown analysis using approximate or arbitrary morphology-based models, this research provides a practical way to generate more representative models by using SEM images of the material to capture its morphology. The agreement between experimental and simulation data supports the validity of the proposed approach, whereas some parameter sensitivity analyses were also provided in the analysis. This article is organised as follows:

Section 2 summarises the properties of the experimental paper samples used to provide data needed to support the development of the model. It also shows the experimental details for the electrical breakdown strength measurement. Section 3 summarises the SEM image-based modelling and simulation methods. Based on this method, cellulose-based materials with varied constituents are modelled and analysed. Section 4 provides the discussion, and the conclusions are summarised in Section 5.

2 | The BN Paper Morphology and Properties

Paper samples used in this study included commercial paper, control paper and novel BN papers as listed in Table 1. The details of the design and fabrication of the laboratory paper samples are given in Ref. [5]. All laboratory papers were made of commercial kraft softwood fibres with Klason lignin content of 3.6%, A.S. Lignin content of 4.3%, Glucan content of 65%, Xylan content of 9.6% and Mannan content of 6.6%. The kraft fibres were first screened to remove knots and then refined to a Canadian Standard Fineness (CSF) 120 mL [23]. 'Control' designates the laboratory control paper having a grammage of 60 g/m^2 (gsm) without BN particles and lignocellulose microfibrils (LCMF). The LCMF was made from the same wood fibres as described previously [24]. 'Control$_{LCMF}$' is another 60 gsm laboratory control paper with the substitution of 15 weight percentage (wt%) of the fibres by LCMF. 'Commercial$_{125gsm}$' is Weidmann (Weidmann Electrical Technology AG, Rapperswil, Switzerland) kraft insulation paper (non-thermally upgraded) with a grammage of 125 g/m^2, whereas 'Commercial$_{76gsm}$' is a thinner commercial Weidmann paper with a grammage of 76 g/m^2 in the same category. 'Commercial$_{35gsm}$' is a lower grammage Weidmann insulation paper of 35 g/m^2 and it has less fibre density of 0.7 g/cm^3 instead of 1 g/cm^3. For paper samples containing BN, 'CSF120LCMF$_{15wt\%}$' stands for the BN paper made from CSF 120 refined fibres and containing 15 wt% LCMF to improve the paper tensile strength. The subscript text label, 'aBN' describes the BN type, that is, agglomerated BN of 25 μm nominal diameter. The wt% after 'aBN' indicates the quantity of BN introduced as a weight percentage of the entire paper.

Typical cross-sectional SEM images of the control and CSF120LCMF$_{15wt\%}$aBN$_{43wt\%}$ samples can be observed in Figure 1. The morphology of the control paper contains voids and fibres in Figure 1a. BN regions can be clearly identified in

TABLE 1 | Names of paper types assessed with their detailed descriptions.

Sample name	Description
Control	60 gsm and made of CSF 120 refined pulp fibre
Control$_{LCMF}$	60 gsm and made of 85 wt% CSF 120 refined pulp fibre with 15 wt% of LCMF
Commercial$_{125gsm}$ Commercial$_{76gsm}$	Weidmann insulation paper with 1 g/cm^3 paper density and different thickness/grammage, 76 gsm and 125 gsm, respectively
Commercial$_{35gsm}$	Weidmann insulation paper with lower paper density of 0.7 g/cm^3 and 35 gsm
CSF120LCMF$_{15wt\%}$ aBN$_{21wt\%}$	BN paper made of CSF 120 refined fibre with 15 wt% of LCMF substitution at fibre grammage of 60 gsm, plus agglomerated BN particles at 21 wt% of the entire paper weight
CSF120LCMF$_{15wt\%}$ aBN$_{30wt\%}$	BN paper made of CSF 120 refined fibre with 15 wt% of LCMF substitution at fibre grammage of 60 gsm, plus agglomerated BN particles at 30 wt% of the entire paper weight
CSF120LCMF$_{15wt\%}$ aBN$_{43wt\%}$	BN paper made of CSF 120 refined pulp fibre with 15 wt% of LCMF substitution at fibre grammage of 60 gsm, plus agglomerated BN particles at 43 wt% of the entire paper weight

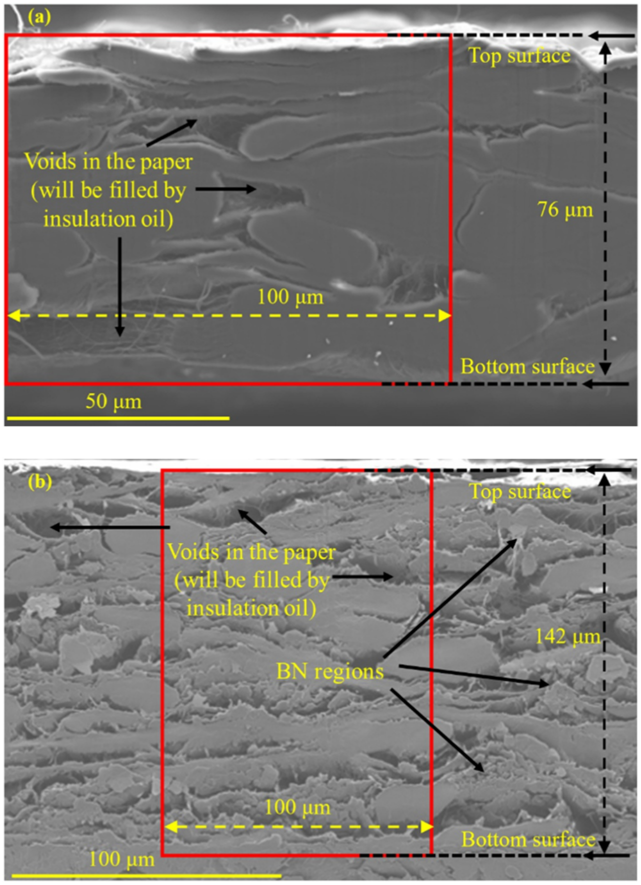

FIGURE 1 | SEM image showing the cross-sectional paper structure. (a) Control paper (b) BN paper-CSF120LCMF$_{15wt\%}$aBN$_{43wt\%}$. The 100 µm wide regions highlighted by the red boxes in both images are applied for the SEM image-based modelling and simulation demonstration in later sections.

the BN paper from the top surface to its bottom in a layered structure separated by lignocellulosic fibres as shown in Figure 1b. Voids are represented by the black areas in both SEM images as paper is a porous material. These voids can be filled by insulation oil during the oil-impregnation process. The oil-impregnation process should be completed before measurements of paper properties, so the oil-impregnated paper samples under measurements can match transformer operating conditions. The 100 µm wide regions marked in both SEM images are used for the SEM image-based modelling and simulation demonstration in Section 3.

Paper samples were prepared following conventional protocols to produce oil-impregnated samples for thermal, mechanical and dielectric characterisation [25]. Specifically, the natural ester insulation oil was dried under vacuum at 115°C for 18 h, whereas the fresh paper samples were dried separately under atmospheric pressure at 105°C for 3 h. Dried paper samples were then impregnated with the dried natural ester insulation oil. During the oil-impregnation process, the paper samples were soaked in the oil under vacuum until air bubble formation subsided, and then kept for another 12 h, to remove any remaining air and moisture.

The dielectric performance of the oil-impregnated insulation paper samples was measured by using an electrode system according to an IEC standard [26]. The electrode dimensions with detail are shown in Figure 2. The diameters of the stainless-steel high voltage electrode and ground electrode are 25 and 75 mm, respectively, with a corner rounding radius of 3 mm. The top and bottom surfaces were polished, flat, and had parallelism within 5 µm. Thus, the interelectrode space during experiments and measurements was controlled by the insulation paper thickness and paper surface roughness, with minimal uncertainty added by the electrode system.

Tapped holes on the electrodes for reliable electrical connections and two slots on the ground electrode to permit the attachment of the ground wire were added as shown in Figure 2. Three measurement slots with controlled horizontal surfaces were added on the high voltage electrode, separated by 120°. The bottom horizontal surfaces of these slots were flat and parallel with the bottom surface of the high voltage electrode. Fowler Quadra test indicators (Part Number 54-562-888) were simultaneously applied to each of the three measurement slots for measuring the interelectrode spacing after inserting the insulation paper coupon. This measurement system can achieve a resolution of 1.27 µm with uncertainty less than 5 µm.

Two replicate electrode systems were used in this study to support data acquisition. One system was only used for high voltage testing, whereas the other was only used for paper sample thickness measurements and some dielectric property

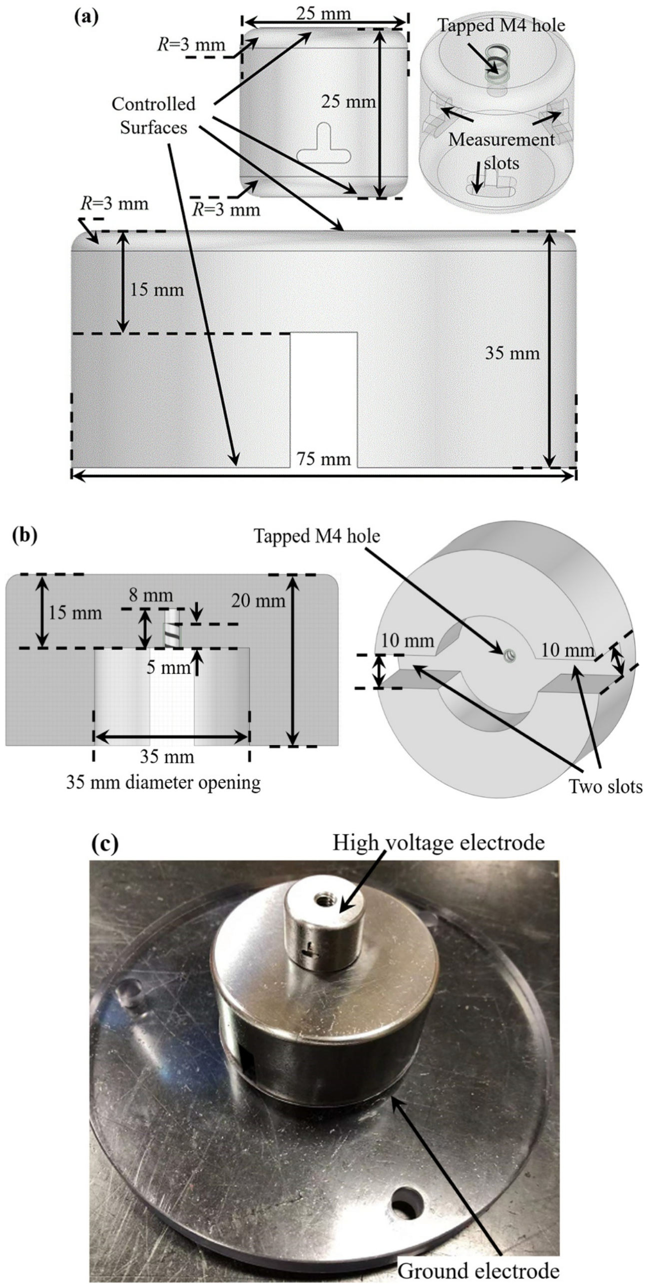

FIGURE 2 | Electrode system applied in this study. (a) Side view of the parallel plate electrodes and the aero view of high voltage electrode with design details (b) Ground electrode with design details (c) Aero view of the fabricated electrodes used in experiments and measurements.

evaluation under low voltage conditions. The breakdown strength measurements of oil-impregnated paper samples under parallel-plate electrodes were performed at 60 Hz and a voltage ramping rate of 750 V/s [26]. A two-parameter Weibull distribution was selected to fit the results and obtain fitting parameters [27].

The three types of BN paper all had greater electrical breakdown strength than both the control and the commercial paper as shown in Figure 3. The commercial paper with higher paper density and thinner paper thickness reached a greater electrical breakdown strength as expected than the paper with lower density or greater thickness. The results also showed that the substitution of LCMF (~15 wt%) had an insignificant effect on the paper electrical breakdown strength. The slopes of the Weibull distribution curves shown in Figure 3a are important to assess sample uniformity and their differences at certain cumulative failure probability. Practical applications, however, focus on avoiding electrical breakdown. Consequently, a safety margin, typically based on the 1% probability of failure, is selected [28]. BN paper samples also had greater electrical breakdown strength at the 1% cumulative breakdown probability as shown in Figure 3b.

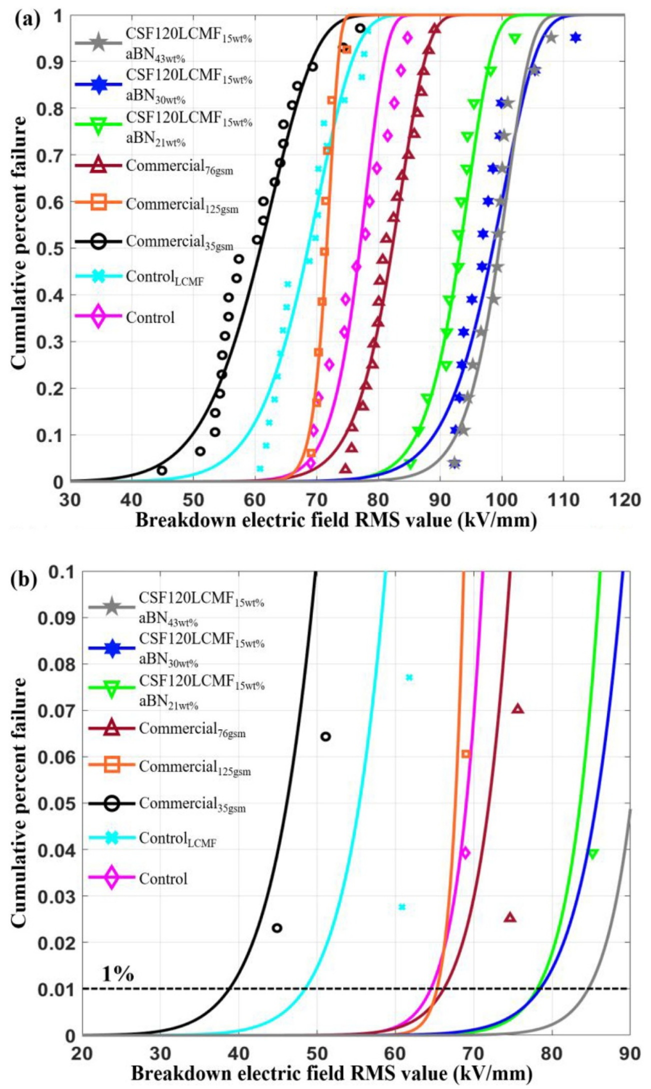

FIGURE 3 | Dielectric strength measurement results for all the paper samples (a) Electrical breakdown strength for commercial, control and BN paper at different cumulative failure rates after the two-parameter Weibull distribution fitting (b) Electrical breakdown strength for commercial, control and BN paper in a low cumulative probability of failure region (0%–10%).

The relative permittivity values of the control, commercial and BN paper were measured at 60 Hz and reported in Table 2. Because the relative permittivity value of cellulose (~6.1) is much higher than BN (~3.9) and insulation oil (~3), the BN paper shows a lower relative permittivity than the control and

TABLE 2 | Relative permittivity of control, commercial and BN paper.

Name	Relative permittivity at 60 Hz AC	
	Average value	Standard deviation
Control	4.5	0.09
$Control_{LCMF}$	4.6	0.25
$Commercial_{125gsm}$	5.5	0.18
$Commercial_{76gsm}$	5.4	0.29
$Commercial_{35gsm}$	3.6	0.23
$CSF120LCMF_{15wt\%}$ $aBN_{21wt\%}$	3.8	0.13
$CSF120LCMF_{15wt\%}$ $aBN_{30wt\%}$	3.8	0.09
$CSF120LCMF_{15wt\%}$ $aBN_{43wt\%}$	3.7	0.05

high-density commercial paper [29–31]. Also, the high-density commercial paper has a higher relative permittivity value than the low-density commercial paper, due to a greater fraction of fibres in the oil–cellulose insulation system.

3 | Electrical Breakdown Strength Analysis via SEM Image Based Modeling and Simulation Method

The prediction of electrical breakdown strength is complex for materials with multiple components such as the oil–BN–cellulose system. It requires understanding of the electric-field distribution and electron dynamics. It also depends on the bulk and interfacial properties of the oil, cellulose and BN as well as the sample morphology. A foundation for developing a more comprehensive modelling approach is the determination of the electric field distribution, which requires a morphology-based model. As shown in Figure 4, an approach to characterise the morphology of an oil–cellulose system can be developed based on SEM imaging.

After identifying the boundaries of different constitutes, commercial software tools such as AutoCAD and Ansys SpaceClaim can be used to further determine the morphology. The same approach can be used for three component systems, for example, an oil–BN–cellulose system as shown in Figure 5. For simplification, the small black regions (voids) in and near the chunk BN particle region were ignored. Similarly, small LCMF fibrils were not identified by the tool, although these fibrils and small voids can be identified by adjusting image contrast or resolution and further training the AI-based tool (segment anything model). The model accuracy can be improved by including more small features identified by SEM, but at the cost of more computational resources and increasing modelling difficulties.

The dielectric strength and relative permittivity of cellulose, natural ester insulation oil and BN particles are important to significantly influence the overall dielectric strength of the hybrid insulation system under 60 Hz AC excitation. For the

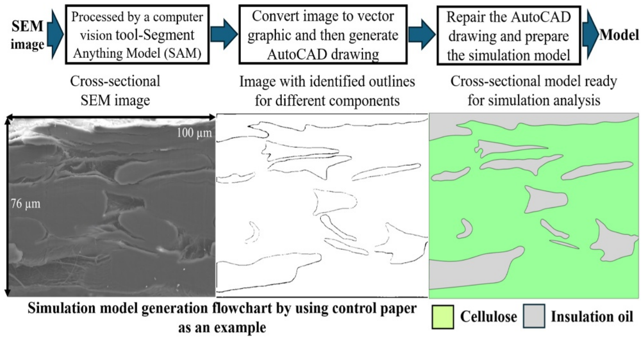

FIGURE 4 | The SEM image-based modelling approach illustrated using the control paper as an example.

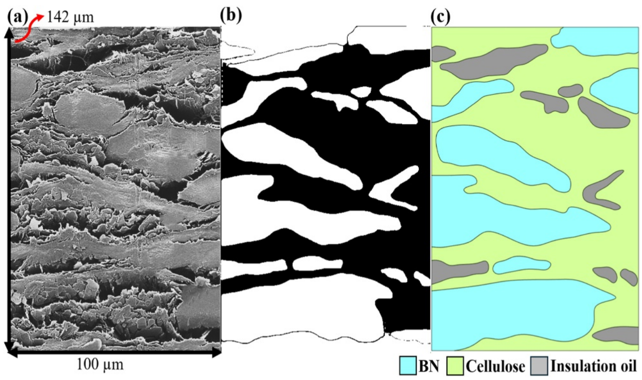

FIGURE 5 | BN paper model generation. (a) Cross-sectional SEM image. (b) Image after segment anything model (SAM) identification. (c) Morphology-based simulation model.

natural ester insulation oil, the dielectric breakdown strength ranges from approximately 15 to 40 kV/mm [31, 32]. When the electric field stress is between 30 kV/mm and 40 kV/mm, the breakdown probability of the insulation oil is above 70%. Thus, 32.5 kV/mm is selected in the simulation according to the product datasheet (Cargill FR3 fluid, natural ester transformer oil) and references under the assumption that electrical breakdown should occur in most oil-filled voids under such electrical stress.

The reported variability in the relative permittivity of the insulation oil is low, ranging from 3 to 3.2 under room temperature, line frequency excitation and very low moisture content. Relative permittivity of 6.1 was reported for cellulose fibres [29]. It is therefore reasonable to assume that the relative permittivity ranges from 5.5 to 6.5, considering that the effects of temperature and moisture are not studied here.

The measurements of the dielectric breakdown strength of pure cellulose, a porous material, are difficult. 138 kV/mm with a standard deviation of 6.2 kV/mm was used in an earlier study [28]. It was found that the dielectric strength of cellulose material is highly dependent on the pore size in cellulose films or nanopapers (films made of cellulose nanofibrils) for energy storage or water filtering applications [33, 34]. Nanopaper with small pore size can exhibit a high dielectric strength, over 200 kV/mm, suggesting the great intrinsic dielectric strength of cellulose. When the pore size of the paper became less than

3 nm, the dielectric strength of nanopaper reached 500 kV/mm [34]. Based on this information, the dielectric strength of 100 kV/mm was selected for cellulose in this study, and a range from 70 to 130 kV/mm was used for the parametric sensitivity assessment in the later section.

The product datasheet (Part No. PTX25, Momentive Technology, Strongsville, USA) indicated a relative permittivity of the BN particles of 3.9, whereas a range between 4 and 4.5 was also widely reported for similar BN material [30].

The intrinsic dielectric strength of BN particles was examined in references [35, 36]. Although the dielectric strength of the BN material is dependent on several factors such as the mechanical stress on the BN particles, reported values were greater than 5 MV/cm (500 kV/mm) [35, 36]. Thus, 500 kV/mm is selected for this study. Because the dielectric strength of BN is much higher than the cellulose and insulation oil, the breakdown path should always occur in the cellulose and oil regions before the breakdown of BN is initiated.

The ranges of the dielectric strength and relative permittivity parameters for cellulose, natural ester insulation oil and BN are summarised in Table 3.

Consistent with the assumption in earlier research [15, 16, 18], the insulation oil reaches its breakdown strength at a lower applied voltage than any other materials in the system in the proposed 2D model as the excitation voltage increases. Thus, oil regions were the first to exceed their breakdown strength under the test conditions. Upon the initiation of partial discharge (PD) in the oil, these regions can be considered as floating conductors that recalibrated the electric field distribution in the remainder of the sample outside of the oil regions [37]. The electric field distribution was calculated by assigning floating electric potentials to the boundaries of the oil regions. A boundary element computational method was used here for its robust performance [38]. In applying the boundary element method, the floating electric potential was achieved by requiring the unknown boundary charge of the subject region to be zero.

Based on the redistribution of the electric field upon discharging in the oil regions, probable electrical breakdown paths can be identified when the excitation voltage reaches the breakdown strength. For the control paper in the oil–cellulose system, a calculated path along which the electric field strength exceeded the electrical breakdown strength of the cellulose and insulation oil is shown in Figure 6. A similar analysis was applied to a representative unit of the BN paper, and an electrical breakdown path is identified in Figure 7.

TABLE 3 | Dielectric strength and relative permittivity parameters range for natural ester oil, cellulose, and boron nitride.

Name	Relative permittivity under 60 Hz AC	Dielectric strength (kV/mm)
Natural ester oil	3 to 3.2	30 to 40
Cellulose	5.5 to 6.5	70 to 130
Boron nitride	3.9 to 4.5	> 500

By comparing Figure 6 with 7, the simulation of the electric field distribution showed that the BN particles decreased the electric field stress in the oil-filled voids, which resulted in an increase in electrical breakdown voltage even though the oil breakdown strength is unchanged. This is consistent with the measured data. For example, at 43 wt% BN loading, the electrical breakdown strength was enhanced by approximately 20% above that of the control paper based on experiments, in agreement with the 30% increase based on simulations. Such agreement supports the validity of the modelling approach despite some differences exist between the simulations and measurements. The differences between the simulated and experimental results can be majorly attributed to several factors, such as differences between the measured morphology and the morphology at the electrically weakest point in the samples, the accuracy of the model, and the uncertainties in the simulation parameters. During the modelling and simulation, it assumes that the voids exist in the dry paper samples are all filled by the insulation oil after the oil-impregnation process for simplification. In fact, partial impregnation may exist, which would reduce the effective breakdown strength of the oil-cellulose system.

To verify the consistency of the proposed modelling approach, another pair of SEM images from different paper samples was analysed. 2D modelling of the control paper and BN paper is carried out accordingly by using the selected pair of SEM images and the same methodology, whereas the modelling results as demonstrated in Figures 8 and 9.

The probable breakdown paths along the oil and cellulose regions are presented in Figure 10a,b for the control and the

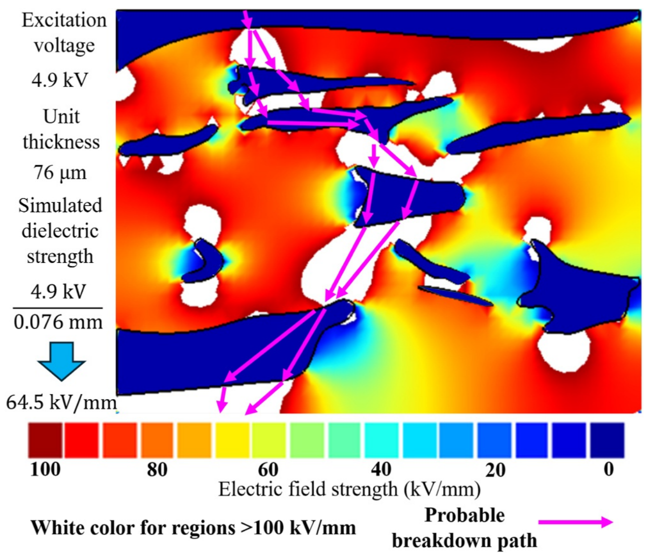

FIGURE 6 | Electric field redistribution after the occurrence of partial breakdown in the insulation oil regions. The E-field strength is sufficient to initiate electrical breakdown in cellulose shown by the white areas. Pink arrows indicate probable breakdown paths as the schematic representation. This control paper model is generated from Figure 4.

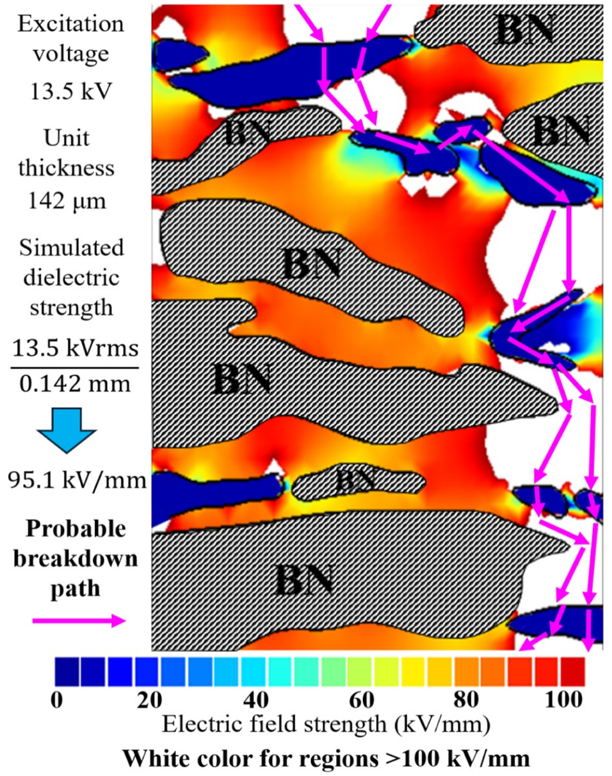

FIGURE 7 | E-field redistribution after the occurrence of partial breakdown in the insulation oil regions. The electric field strength is sufficient to initiate electrical breakdown in the cellulose shown by the white areas, and probable breakdown paths are identified by the pink arrows as the schematic representation. This BN paper model is generated from Figure 5.

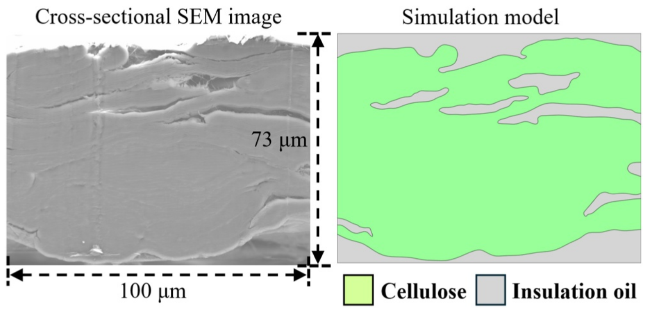

FIGURE 8 | Another example for control paper model generation: Cross-sectional SEM image and the morphology-based simulation model.

BN paper, respectively. In this example, under 43 wt% BN loading, the electrical breakdown strength was enhanced by approximately 30% based on simulations, which is similar to the enhancement from previous example as shown in Figures 6 and 7. Comparing these results with the previous examples in Figures 6 and 7, the predicted electrical breakdown strengths of the control and BN paper from these examples were approximately 9% and 5% lower, respectively. The small variations in the predicted electrical breakdown strengths between these two sets of examples suggest that the modelling approach adopted in the study is reliable for providing consistent results.

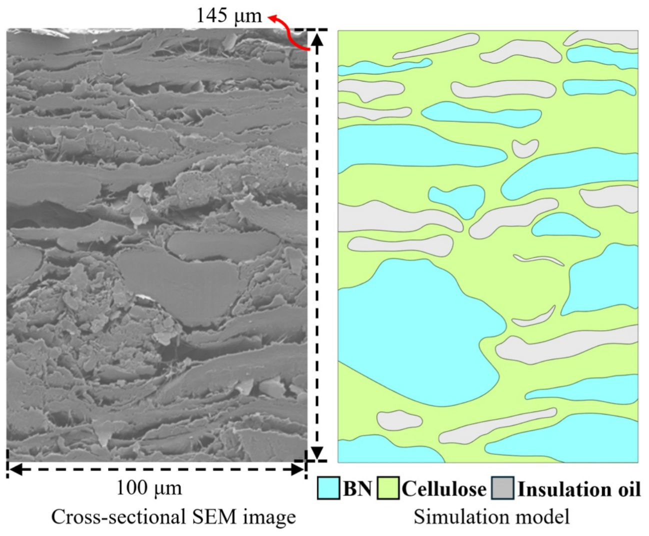

FIGURE 9 | Another example for BN paper model generation: Cross-sectional SEM image and the morphology-based simulation model.

Parametric sensitivity analysis was applied to the pair of paper samples shown in Figures 8 and 9. According to Table 3, two sets of parameters are selected that represent the lowest and highest dielectric strength estimations of the hybrid system as listed in Table 4.

4 | Discussion

Exploiting SEM images, the modelling approach demonstrated in this study introduces 2D morphology mapping to guide insulation performance interpretation and estimate regions where 3D mapping might be necessary. As a practical morphology-based modelling first proposed here for dielectric strength analysis of a hybrid insulation system, this 2D method provides insights into the measured 3D phenomena.

Breakdown is a 'weak link' phenomenon, that is, it occurs at the weakest point, not a point of average strength. The narrow spread in the Weibull distributions of the experimental breakdown data shown in Figure 3a suggests that the variabilities among paper samples were small, despite the variations in paper sample morphology. This suggests that the morphology variation had limited influence on dielectric strength of the hybrid insulation system studied here.

The utility of the present modelling approach is further supported by the examples given in Figures 4, 5, 8, and 9. Although the simulated morphologies in Figures 8 and 9 seemed quite different from those in Figures 4 and 5, the variations in the predicted electrical breakdown strengths, however, were quite small, only approximately 5%–10% for the control and BN paper, respectively. For parametric sensitivity analysis, when the simulation parameters are selected in a reasonable range, it confirms that BN paper had an approximately 20%–30% higher dielectric strength than that of the control paper regardless of the absolute simulation values, further supporting the utility of the modelling approach.

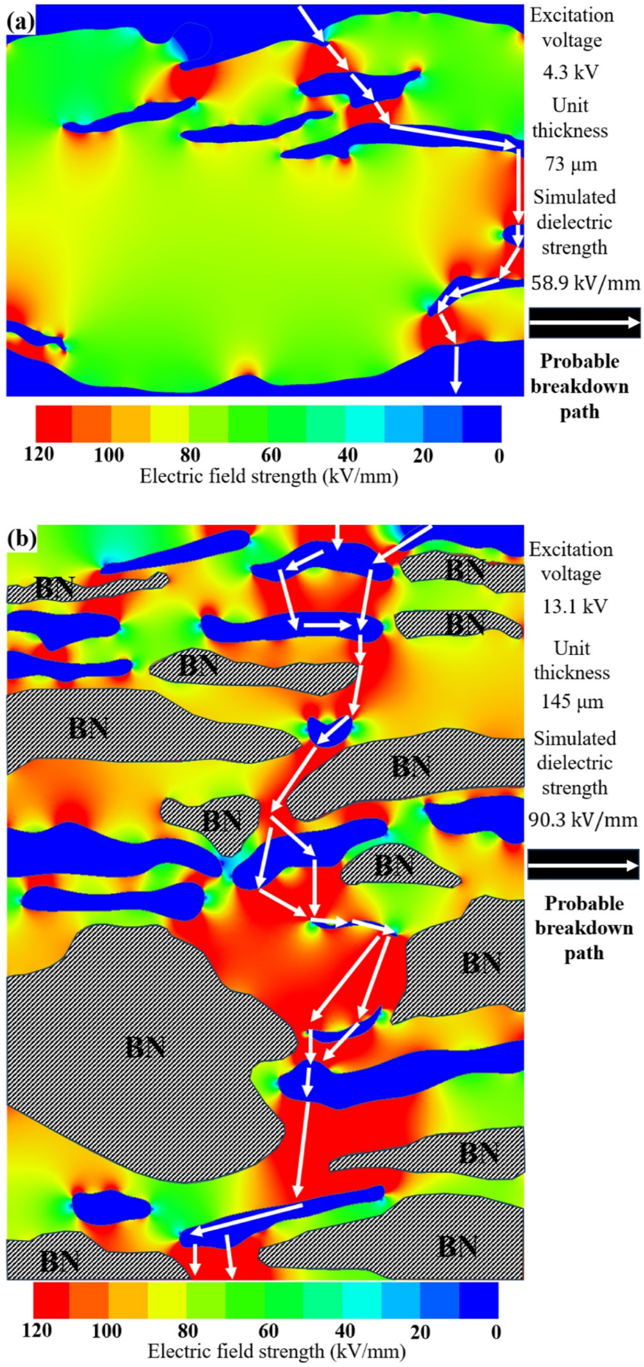

FIGURE 10 | Identification of probable breakdown paths and prediction of dielectric strength for (a) control paper modelled in Figure 8 and (b) BN paper modelled in Figure 9.

3D modelling of porous media via micro-CT has been applied to other material systems, such as concrete, to evaluate its thermal and mechanical properties [39–42]. Based on the promising results from 2D modelling demonstrated here, 3D modelling is warranted in future studies for better describing the hybrid insulation system via advanced computational tomography technology.

This study investigated the short-term dielectric breakdown phenomena, and all experimental data were obtained by using fresh samples under room temperature, low moisture level (almost moisture free) and 60 Hz AC excitation based on the standards [25, 26]. The quantification of longer-term ageing effects, for example partial discharges, cellulous deterioration, moisture effects, space charge, etc., is an important task for ongoing and future research.

5 | Conclusion

This research advanced modelling for electrical breakdown analysis of the oil–cellulose and oil–BN–cellulose systems. Improving modelling is a key capability needed to understand the mechanism for advancing optimal material design to support the design and development of materials, which are well engineered for specific electric, mechanical and thermal environments.

This investigation shows that the SEM imaging can be used to generate a two-dimensional paper morphology map which can further provide reasonable simulation results. It would be interesting to verify whether the method proposed here can be applied to other insulation systems such as polymers with fillers, which need more research effort in the future.

The simulation results suggest that micro-scale BN particles changed the electric field distribution to result in a decreasing electric field strength in the oil-filled voids at a given voltage. Moreover, compared with cellulose, a BN particle can take more electric stress before its breakdown due to its lower relative permittivity and higher dielectric strength.

Simulations from two sets of paper samples showed consistent results in agreement with the experimental data, however, more analyses may be needed in the future to determine the error bars of the simulation results with more inputs and case studies by using large numbers of SEM images.

The analysis method together with the simulation results showed a failure mechanism that is different from that in polymeric systems in which the voids are air filled [13, 38, 43]. In polymeric systems, repeated partial discharges in voids weakens the surrounding polymer and stimulates void growth. In this study, partial discharges in the oil-filled voids changes the electric field distribution in the rest of the insulation system, which then triggers the electrical breakdown. Given the higher density of oil than air, the mean free path of electrons in oil is significantly less than that in air. As a result, electrons gain less energy from collisions in oil than in air, and thus can decrease the energy available for plasma etching.

Also, for the polymeric system, the extensive loading of fillers can increase the system viscosity and lead to more air voids after being cured, which significantly decreases the electrical breakdown strength of the entire system. By comparison, the voids introduced between the fillers and cellulose-based matrix in this study can be filled by insulating oil after proper oil impregnation, so the breakdown strength of the oil–BN–cellulose system did not decrease with increasing BN filler loading.

Moreover, for polymeric systems, the relative permittivity value of the fillers is typically higher than the polymer matrix. Thus,

TABLE 4 | Parametric sensitivity analysis of the control paper and BN paper based on the models in Figures 8 and 9, respectively.

Simulation parameter selection				
	Case 1 (to generate the lowest dielectric strength of the hybrid material system)		Case 2 (to generate the highest dielectric strength of the hybrid material system)	
Material	Relative permittivity	Dielectric strength (kV/mm)	Relative permittivity	Dielectric strength (kV/mm)
Natural ester oil	3	30	3.2	40
Cellulose	5.5	70	6.5	130
Boron nitride	4.5	500	3.9	500

Simulated dielectric strength of the hybrid material system with different parameter selection		
Material	Lowest predicted dielectric strength of the hybrid system by using parameters in Case 1	Highest predicted dielectric strength of the hybrid system by using parameters in Case 2
Control paper	39.7 kV/mm	71.2 kV/mm
BN paper	58.6 kV/mm	106.9 kV/mm

the electric stress is enhanced in the polymer matrix instead of the fillers [13]. However, for cellulose-based matrix, thanks to the higher relative permittivity value of the cellulose, more electric stress can be shifted to fillers from the cellulose, which generates favourable electric field distribution and helps avoiding the formation of probable electrical breakdown paths, as verified by the simulation results. The results can be different with fillers of different properties, especially when the fillers have high relative permittivity values.

The results constitute a promising advance in the ability to model oil-impregnated insulation paper systems with fillers. This research improves the modelling of morphology and the exploration of physics for the insulation failure in such systems. The morphology-based modelling and the analysis method can support the development of better insulation paper for specific applications, such as power transformers, to help extend the transformer life and meet the requirements of the power utility today for better reliability and resilience.

Acknowledgements

The authors thank Cargill (Kevin R. Wirtz), Weidmann (George Doyle and Aleksandr Levin) and Momentive Technologies (Xiang Bei) for the information on the materials used. Roland Gleisner and John Considine at the USDA Forest Products Lab, Madison, Wisconsin for their help and advice on handsheet fabrication. Alan Sbravati, Camden Spiller, David Wallach, Samuel Sharpless, Sheldon Kennedy, Bruce Forsyth, Phil Hopkinson, Amitabh Sarka, and Rajiv Kuma for their advice on transformer technology and use, and J. Hahne and B. Morrison for design and assembly of test apparatus. Congxi Zhang, Oliver Wang and Dr. Xianyong Feng for their help on the samples' properties measurement. Dr. Meiling Wu at University of Maryland for her help on the initial explorations of the laboratory paper fabrication and evaluation. The findings and conclusions in this study are those of the authors and should not be construed to represent any official USDA or U.S. government determination or policy.

Funding

This study was supported by Advanced Research Projects Agency-Energy (ARPA-E) (Grant No. DE-AR0001392).

Conflicts of Interest

The authors declare no conflicts of interest.

Data Availability Statement

The data that support the findings of this study are available from the corresponding author upon reasonable request.

References

1. S. Bilyaz, A. Bhati, M. Hamalian, et al., "Modeling the Impact of High Thermal Conductivity Paper on the Performance and Life of Power Transformers," *Heliyon* 10, no. 6 (2024): e27783.

2. M. Lokanathan, P. V. Acharya, A. Ouroua, S. M. Strank, R. E. Hebner, and V. Bahadur, "Review of Nanocomposite Dielectric Materials With High Thermal Conductivity," *Proceedings of the IEEE* 109, no. 8 (2021): 1364–1397.

3. M. Luo, Y. Zhou, R. Wang, X. Cao, and Z. Wang, "Enhanced Dielectric Breakdown Strength and Thermal Conductivity of Silicone Gel Composites With High-Electron-Affinity Silicon Dioxide/Cationic Polymer/Nano-Diamond," *Chemical Engineering Journal* 501 (2024): 157623.

4. Y. Zhou, X. Tian, X. Cao, et al., "Enhanced Thermal Conductivity and Electrical Insulation Properties of Liquid Crystalline Epoxy Composites by Using Optimized Alumina Hybrid Fillers," *Materials Today Physics* 54 (2025): 101719.

5. Y. Xu, T. Soori, Q. Zhang, et al., "Boron Nitride Enhanced Electric Insulation Paper for Extending Transformer Thermal Life," *Materials & Design* 254 (2025): 114112.

6. L. S. Schadler, J. K. Nelson, C. Calebrese, A. Travelpiece, and D. L. Schweickart, "High Temperature Breakdown Strength and Voltage Endurance Characterization of Nanofilled Polyamideimide," *IEEE Transactions on Dielectrics and Electrical Insulation* 19, no. 6 (2012): 2090–2101.

7. L. S. Schadler and J. K. Nelson, "Polymer Nanodielectrics—Short History and Future Perspective," *Journal of Applied Physics* 128, no. 12 (2020): 120902.

8. B. X. Du, X. L. Li, J. Li, and X. Y. Tao, "Effects of BN Nanoparticles on Thermal Conductivity and Breakdown Strength of Vegetable Oil," in *2015 IEEE 11th International Conference on the Properties and Applications of Dielectric Materials (ICPADM)* (2015), 476–479.

9. C. Chen, M. Niu, L. Wang, et al., "Effect of Nanoparticle Type on Prebreakdown and Breakdown Characteristics of Transformer Oil," in *2018 IEEE 2nd International Conference on Dielectrics (ICD)* (2018), 1–4.

10. G. Qu, H. Cui, Y. Zhu, L. Yang, and S. Li, "Substantial Improvement of the Dielectric Strength of Cellulose–Liquid Composites: Effects of Traps at the Nanoscale Interface," *Journal of Physical Chemistry Letters* 11, no. 5 (2020): 1881–1889.

11. C. Tang, S. Zhang, J. Xie, and C. Lv, "Molecular Simulation and Experimental Analysis of Al_2O_3-Nanoparticle-Modified Insulation Paper Cellulose," *IEEE Transactions on Dielectrics and Electrical Insulation* 24, no. 2 (2017): 1018–1026.

12. R. Liao, C. Lv, L. Yang, Y. Zhang, W. Wu, and C. Tang, "The Insulation Properties of Oil-Impregnated Insulation Paper Reinforced With Nano-TiO_2," *Journal of Nanomaterials* 2013, no. 1 (2013): 373959.

13. C. Zhang, J. Xiang, S. Wang, et al., "Simultaneously Enhanced Thermal Conductivity and Breakdown Performance of Micro/Nano-BN Co-Doped Epoxy Composites," *Materials* 14, no. 13 (2021): 3521.

14. E. F. Kelley and R. E. Hebner, "Electro-Optic Measurement of the Electric Field Distribution in Transformer Oil," *IEEE Transactions on Power Apparatus and Systems*, no. 7 (1983): 2092–2097.

15. M. Kim, R. E. Hebner, and G. A. Hallock, "Modeling the Growth of Streamers During Liquid Breakdown," *IEEE Transactions on Dielectrics and Electrical Insulation* 15, no. 2 (2008): 547–553.

16. M. Huang, Y. Ying, B. Liu, Y. Lv, B. Qi, and C. Li, "Enhanced Voltage Distribution and Breakdown Strength Performances of Oil-Paper Composite Insulation by Adding TiO_2 Nanoparticles," *High Voltage* 6, no. 1 (2021): 42–50.

17. T. Gabler, K. Backhaus, S. Großmann, and R. Fritsche, "Dielectric Modeling of Oil-Paper Insulation Systems at High DC Voltage Stress Using a Charge-Carrier-Based Approach," *IEEE Transactions on Dielectrics and Electrical Insulation* 26, no. 5 (2019): 1549–1557.

18. F. Qin, S. Li, W. Chen, Z. Cui, X. Nie, and W. Wu, "Breakdown Characteristics and Damage Mechanism of Typical Defects in Oil-Paper Insulation Under HEMP," *IEEE Transactions on Dielectrics and Electrical Insulation* (2024).

19. M. Huang, Y. Zhou, Z. Zhou, and B. Qi, "A Combined Electro-Thermal Breakdown Model for Oil-Impregnated Paper," *Energies* 10, no. 12 (2017): 2160.

20. J. H. Shin, D. Olsen, C. Coffelt, L. S. Martin, and M. Zhou, "Dielectric Breakdown of Heterogeneous Materials Under Electromagnetic Pulses," *Journal of Materials Research* 37, no. 23 (2022): 4059–4070.

21. D. Olsen, L. S. Martin, and M. Zhou, "Computational Prediction of Dielectric Breakdown Strength of a Transformer Paper in Oil With Uncertainty Quantification," *Materials Research Express* 11, no. 8 (August 2024): 085508.

22. Y. Lv, Y. Ge, L. Wang, et al., "Effects of Nanoparticle Materials on Prebreakdown and Breakdown Properties of Transformer Oil," *Applied Sciences* 8, no. 4 (2018): 601.

23. ISO Standard, "Pulps—Determination of Drainability—Part 2: 'Canadian Standard' Freeness Method," ISO 5267/2-1980.

24. X. Zhang, P. Kitin, U. Agarwal, R. Gleisner, and J. Y. Zhu, "Characterizing Lignin- Containing Microfibrillated Cellulose Based on Water Interactions, Fibril Properties, and Imaging," *Carbohydrate Polymers* 316 (2023): 1209.

25. ASTM D2413-16, "Standard Practice for Preparation of Insulating Paper and Board Impregnated With a Liquid Dielectric," .

26. IEC 60243-1, "2013 Electric Strength of Insulation Materials: Test Methods—Part 1: Tests at Power Frequencies," .

27. IEC 62539, "2007 Guide for the Statistical Analysis of Electrical Insulation Breakdown Data," .

28. W. Ziomek, K. Vijayan, D. Boyd, K. Kuby, M. Franchek, "High Voltage Power Transformer Insulation Design," in *Electrical Insulation Conference (EIC)* (2011): 211–215.

29. H. A. De Luca, W. B. Campbell, and O. Maass, "Measurement of the Dielectric Constant of Cellulose," *Canadian Journal of Research* 16b, no. 8 (1938).

30. H. Lin, G. Feng, H. Wang, et al., "Effect of BN Addition on Mechanical and Electrical Properties of Oxidative Sintered Porous Si_3N_4-BN Composites," *Ceramics International* 49, no. 22 (2023): 36637–36645.

31. K. Jariyanurat, S. Maneerot, P. Nimsanong, P. Kitcharoen, P. Chaisiri, and N. Pattanadech, "Dielectric Properties of Mineral Oil Compared With Natural Ester," in *2017 IEEE 19th International Conference on Dielectric Liquids (ICDL)* (2017), 1–4.

32. V. P Charalampakos, G. D. Peppas, E. C. Pyrgioti, A. Bakandritsos, A. D. Polykrati, and I. F Gonos, "Dielectric Insulation Characteristics of Natural Ester Fluid Modified by Colloidal Iron Oxide Ions and Silica Nanoparticles," *Energies* 12, no. 17 (2019): 3259.

33. J. Huang, Y. Zhou, Z. Zhou, and R. Liu, "Dramatically Enhanced Electrical Breakdown Strength in Cellulose Nanopaper," *AIP Advances* 6, no. 9 (2016): 095026.

34. Y. Yin, C. Zhang, W. Yu, et al., "Transparent and Flexible Cellulose Dielectric Films With High Breakdown Strength and Energy Density," *Energy Storage Materials* 26 (2020): 105–111.

35. A. Ranjan, N. Raghavan, M. Holwill, et al., "Dielectric Breakdown in Single-Crystal Hexagonal Boron Nitride," *ACS Applied Electronic Materials* 3, no. 8 (2021): 3547–3554.

36. B. Wang, C. Yu, Y. Jiang, et al., "Dielectric Strength Weakening of Hexagonal Boron Nitride Nanosheets Under Mechanical Stress," *Nature Communications* 16, no. 1 (2025): 8078.

37. E. Kelley and R. Hebner, "The Electric Field Distribution Associated With Prebreakdown Phenomena in Nitrobenzene," *Journal of Applied Physics* 51, no. 1 (1981): 191–195.

38. Y. Xu, K. Davey, W. Zhao, R. E. Hebner, and M. Yazdani, "Electric Field Distributions in Laser Drilled Voids of Polymeric Test Samples," *IEEE Access* 12 (2024): 64351–64359.

39. Y. Huang, Z. Yang, W. Ren, G. Liu, and C. Zhang, "3D Meso-Scale Fracture Modelling and Validation of Concrete Based on In-Situ X-Ray Computed Tomography Images Using Damage Plasticity Model," *International Journal of Solids and Structures* 67–68 (2015): 340–352.

40. T. Pak, N. L. Archilha, S. Berg, and I. B. Butler, "Design Considerations for Dynamic Fluid Flow in Porous Media Experiments Using X-Ray Computed Micro Tomography—A Review," *Tomography of Materials and Structures* 3 (2023): 100017.

41. D. Liu, H. Chen, L. A. Chacon, V. M. Ramu, and S. J. Poovathingal, "Micro-CT Image-Based Computation of Effective Thermal and Mechanical Properties of Fibrous Porous Materials," *Composites Part B: Engineering* 281 (2024): 111502.

42. S. Du, D. Li, M. J. Li, and Y. L. He, "Numerical Study on the Effective Thermal Conductivity and Thermal Tortuosity of Porous Media With Different Morphologies," *Science China Technological Sciences* 67, no. 6 (2024): 1685–1694.

43. P. H. F. Morshuis, "Degradation of Solid Dielectrics Due To Internal Partial Discharge: Some Thoughts on Progress Made and Where to Go now," *IEEE Transactions on Dielectrics and Electrical Insulation* 12, no. 5 (2005): 905–913.